Reflection characteristics of a composite planar AMC surface

Ruey-Bing Hwang and Yueh-Lin Tsai

Citation: AIP Advances **2**, 012128 (2012); doi: 10.1063/1.3682352
View online: http://dx.doi.org/10.1063/1.3682352
View Table of Contents: http://scitation.aip.org/content/aip/journal/adva/2/1?ver=pdfcov
Published by the AIP Publishing

Reflection characteristics of a composite planar AMC surface

Ruey-Bing Hwang[a] and Yueh-Lin Tsai
Department of Electrical Engineering, National Chiao Tung University, 1001 Ta-Hsueh Road, Hsinchu, Taiwan

(Received 24 September 2011; accepted 4 January 2012; published online 26 January 2012)

This study investigates the reflection characteristics of a composite Artificial Magnetic Conductor (AMC) surface consisting of multiple orthogonal gradient AMC surfaces arranged in a two-dimensional periodic pattern. The gradient AMC surface in this study consists of square metal patches of variable size printed on a grounded dielectric substrate. Due to the orthogonal placement of the gradient AMC surface, the incident energy of a plane wave normally incident on the composite AMC surface will be reflected into four major lobes away from the impinging direction. To achieve a systematical design, a simple formula based on array antenna theory was developed to determine the reflection pattern of the gradient AMC surface illuminated by a normal incident plane wave. A time-domain full-wave simulation was also carried out to calculate the electromagnetic fields in the structure and the far-field patterns. The scattering patterns of the structure were measured in an electromagnetic anechoic chamber. Results confirm the design principle and procedures in this research. Since such a composite AMC surface can be easily fabricated using the standard printed circuit board technique without via-hole process, it may have potential applications in beam-steering and radar cross section reduction. [doi:10.1063/1.3682352]

I. INTRODUCTION

A perfect electric conductor (PEC) reflects an incident wave with an 180° phase shift, while a perfect magnetic conductor (PMC) can reflect the incident wave in phase. Although PMCs are not known to exist in nature, a surface with high surface-impedance boundary condition, defined as the ratio between the tangential electric and magnetic fields on the surface, can mimic the reflection characteristics of a PMC. Researchers have recently developed some interesting structures with high impedance-surface properties. For example, a periodic mushroom-type texture, called Sievenpiper's mushroom, was implemented using printed circuit board technology. This design was able to suppress the propagation of surface waves. This surface can reflect electromagnetic waves with no phase reversal, behaving as a perfect magnetic conductor.[1] Other researchers developed a wideband AMC structure with its unit cell containing unclosed rectangular loops, four square patches, and a cross in the center.[2] Other research demonstrates several different unit-cell patterns design based on genetic algorithm for multiband AMC surface using high impedance frequency selective surfaces.[3] A thin AMC structure was recently designed and verified for RCS reduction. This structure consists of a combination of AMC and PEC cells using Sievenpiper's mushrooms and full metallic patches, respectively, to form a two-dimensional array on a plane. This design achieves more than a 20 dB reduction of the RCS value with respect to a reference metallic plate for normal incidence.[4] Another study presents an ultra-thin and broadband radar absorbing material based on periodically arranging two different types of thin planar slabs that are both AMCs with different phase characteristics that are arranged in a checkerboard configuration.[5] A chessboard

[a]Electronic mail: raybeam@mail.nctu.edu.tw

reflector composed of simple interlaced pattern of doubly periodic square metal and dielectric patches was also proposed for radar cross-section reduction.[6] Finally, another study presents an absorber consisting of an artificial magnetic ground plane with surface mount resistors interconnecting a textured surface of square patches.[7] Researchers have developed mechanical and electrical tuning methods for tunable AMCs (or high impedance surfaces) by adjusting the resonant frequency of the unit cell. For example, incorporating varactor diodes into the resonant unit cell of the periodic surface texture produces a tunable impedance surface.[8] A mechanically tunable impedance surface was developed to change the resonance frequency of each unit cell and the dispersion relation of the leaky wave, achieving a two-dimensional beam steering.[9] Researchers have also designed a varactor-tunable high impedance surface with a resistive-lumped-element biasing Grid.[10] Previous research on the AMC or high impedance surface can be traced back to the reflectarray antenna design. The input impedance of an open-ended waveguide array terminated with short-circuited boards operated in the dominant mode can be characterized as an impedance surface. Synthesizing the distribution of the surface impedance can obtain a desired phase front for reflecting the incoming wave into a desired direction.[11] A reflectarray antenna using microstrip patches of variable size for controlling their phase distribution was developed.[12] Other researchers developed a Ka-band microstrip reflectarray with identical square patches with identical microstrip phase-delay lines but different element rotation angles.[13] The current study presents an AMC surface implemented using square metal patches printed on a dielectric slab backed with a metal ground plane. Specifically, this study designs a unit cell containing several sizes of patches with the gradient reflection phase distribution. Repeating this gradient unit cell forms a periodically gradient AMC surface. The periodic variation of this structure can increase the RCS reduction by producing narrow beam-width major lobes reflecting away from the broadside direction. Furthermore, the orthogonal placement of the periodically gradient AMC surfaces can produce four major lobes reflecting away from the surface when it is normally incident by a vertical- or horizontal- polarization plane wave. The organization of this paper is given as follows. Section II defines the structure configuration of an AMC surface made up of a 2D metal patches array and introduces the unit cell approach for determining the reflection phase of the AMC surface. Section III investigates the reflection characteristics of a gradient AMC surface containing different sizes of square metal patches, including the phase angle distribution and the far-field pattern. Section IV describes the fabrication of the AMC surfaces and measures their reflection characteristics, including the mono-static and bi-static RCS. Finally, Section V offers some concluding remarks.

II. REFLECTION PHASE OF A 2D PERIODIC STRUCTURE CONSISTING OF METAL PATCHES ARRAY

Figure 1(a) depicts a 2D periodic structure consisting of square metal patches printed on a dielectric substrate backed with metal ground plane. The structure is assumed to be infinite in extent along the x- and y- axis. The periods (unit-cell size) along the x- and y- axis are the same (denoted as d) and are much smaller than that of the operational wavelength. The dimension of the square metal patch in each unit cell is denoted as a. A uniform plane wave is normally incident on the structure with its electric field along the y-axis. Since the period d is assumed to be much smaller than that of the operation wavelength, all the higher-order space harmonics excluding (m=0, n=0) will become evanescent (non-propagation) waves. The propagation constant of the higher space harmonic is given as follows.

$$k_{zmn} = \sqrt{k_o^2 - \left(k_x + m\frac{2\pi}{d}\right)^2 - \left(k_y + n\frac{2\pi}{d}\right)^2}; \quad m, n \in \text{integer} \tag{1}$$

For the normal incidence condition ($k_x = 0$, $k_y = 0$) and the assumption of $\lambda \gg d$, Eq. (1) can be rewritten as

$$k_{zmn} = -jk_o\sqrt{\left(m^2 + n^2\right)\left(\frac{\lambda}{d}\right)^2 - 1}; \quad \text{excluding} \quad (m{=}0, n{=}0) \tag{2}$$

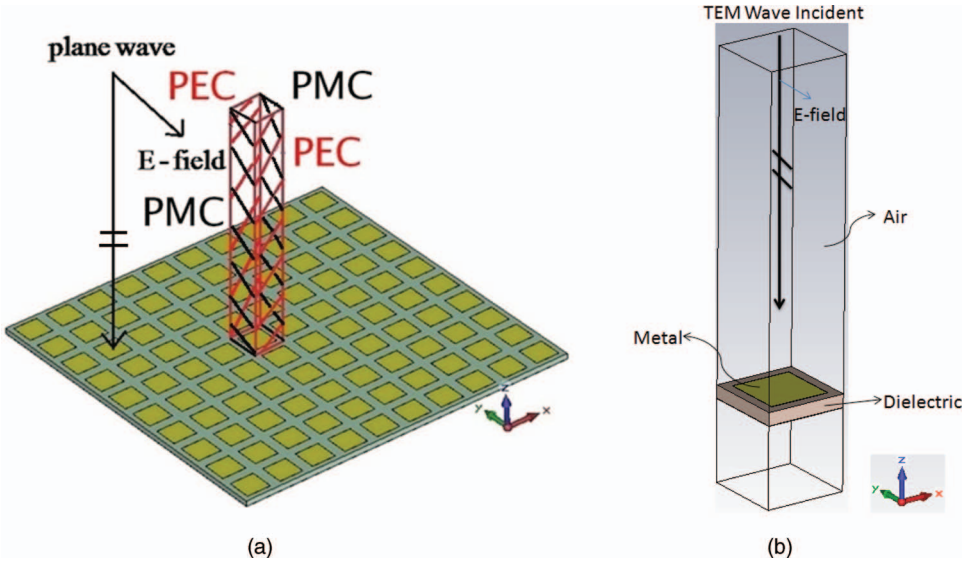

FIG. 1. (a) Structure configuration of an infinite 2D periodic structure and the boundary conditions assignment for the unit cell: normal incident condition. (b) Inhomogeneous media structure in the waveguide used in the simulation.

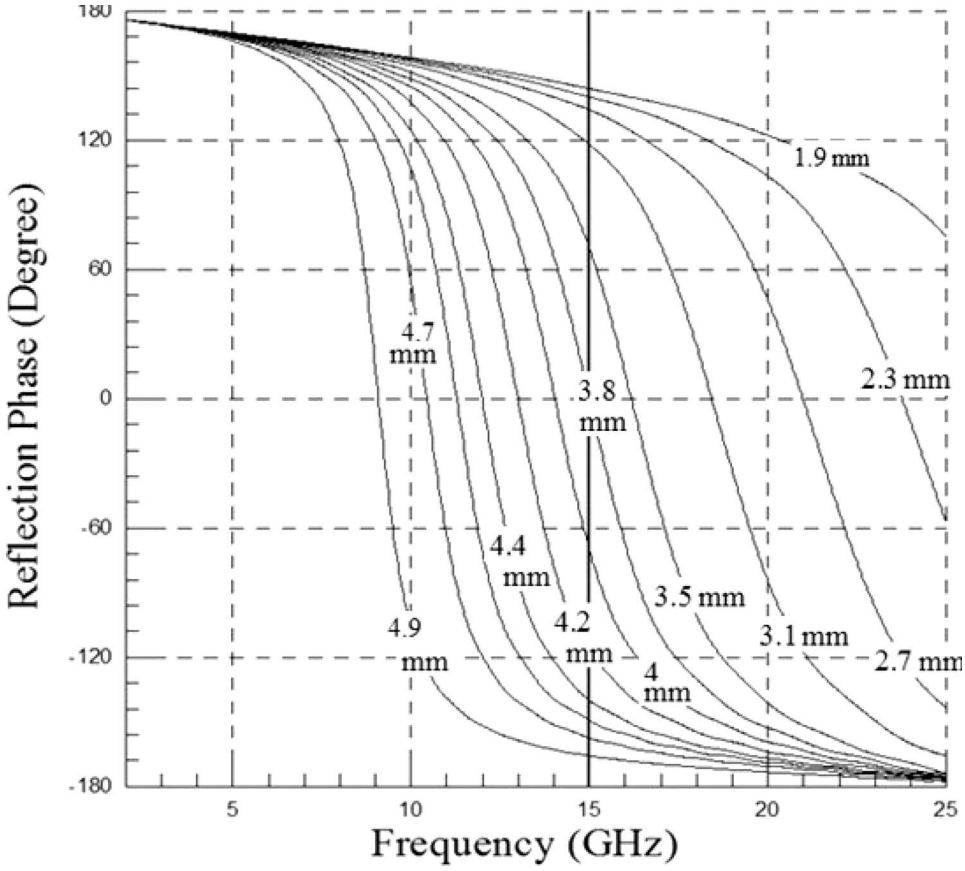

FIG. 2. Variation of the reflection phase versus frequency for various sizes of square metal patches with period d = 5 mm

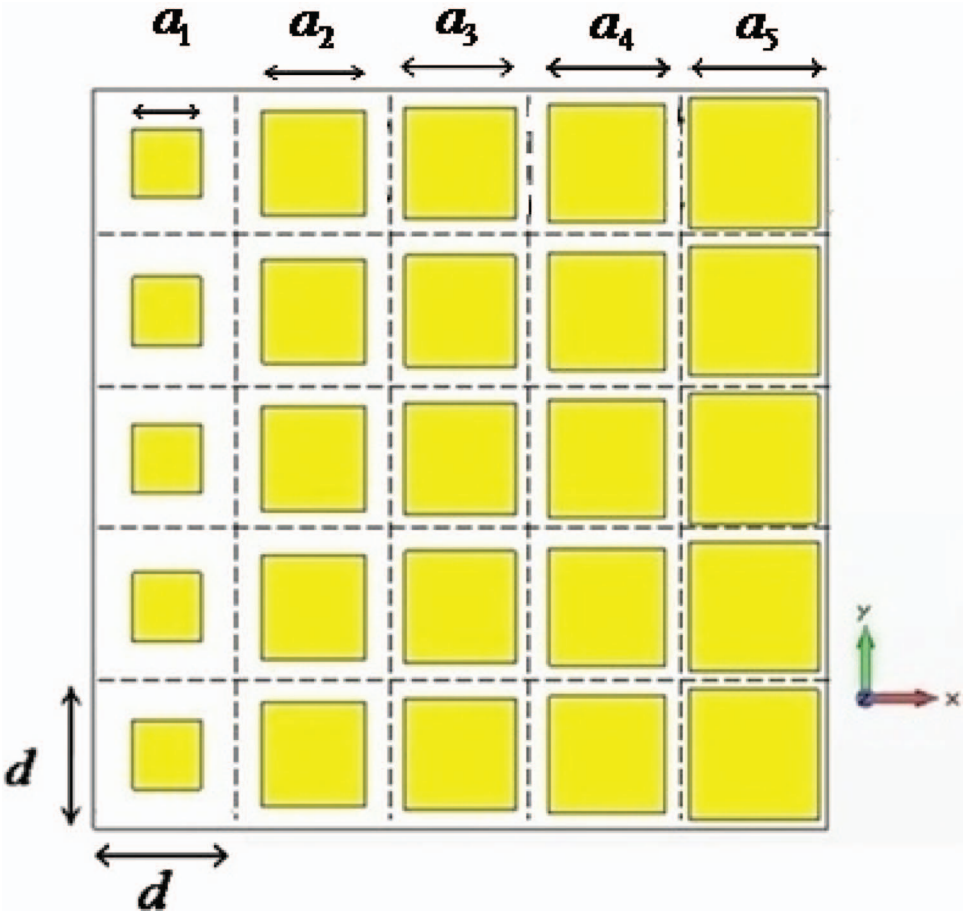

FIG. 3. A gradient AMC surface consists of a 5-by-5 square patches array, d=5mm.

Equation (2) reveals that all the higher-order space harmonics become below-cutoff (evanescent) waves. Therefore, the reflection characteristics of the infinite structure can be determined through the unit cell approach. Due to the normal incidence and electric-field vector along the y-axis, the unit cell is a rectangular tube with the two PEC walls along the y-axis and two PMC walls along the x-axis, respectively (Fig. 1(a)). This problem can be regarded as a waveguide filled with inhomogeneous medium consisting of dielectric, metal, and air regions in the waveguide and terminated by a metal plate on its bottom surface. Subject to the boundary conditions given previously, the fundamental waveguide mode is a TEM wave with its electric and magnetic fields along the y and x axes, respectively (Fig. 1(b)). The reflection amplitude and phase angle can be determined by performing the scattering analysis of the waveguide mode by the discontinuity containing inhomogeneous medium and metal patch. We can also infer the surface impedance by means of the numerical simulation tool to calculate the reflection coefficient Γ and then derive the surface impedance through the relation $\Gamma = \frac{z_s - z_0}{z_s + z_0}$.

Figure 2 shows the reflection phase angle versus frequency for various dimensions of the square metal patch. The vertical and horizontal axes represent the reflection phase angle in degree and the operational frequency in the unit of GHz, respectively. The dielectric substrate employed is FR4, with a relative dielectric constant 4.5 and thickness 0.8 mm. The period is 5 mm. This figure clearly shows that the reflection phase is zero degrees at 15GHz for the case with a patch dimension a = 3.77 mm.

III. REFLECTION CHARACTERISTICS OF A GRADIENT AMC SURFACE

As demonstrated in the previous section, the phase angle of the plane wave reflected by an AMC surface can be adjusted by varying the dimensions of the square metal patch. Therefore, the

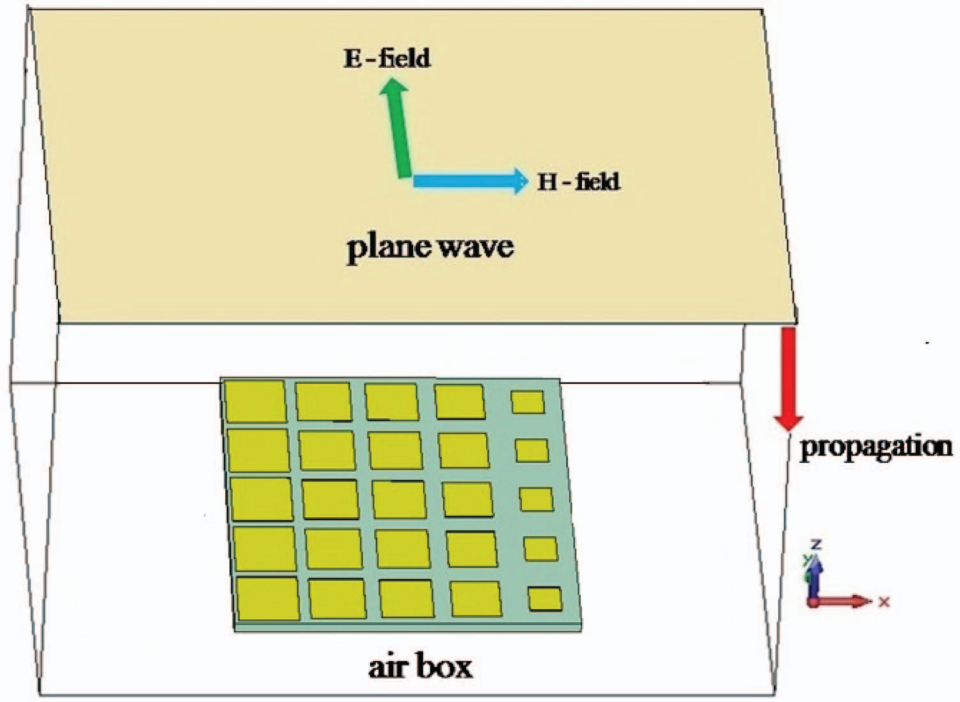

FIG. 4. Environment for full-wave simulation of a gradient AMC surface placed inside a box equipped with absorbing boundary conditions on its walls.

reflection phase on a surface containing various sizes of metal patches should vary with respect to the observation position. For example, Fig. 3 illustrates a 5-by-5 square patch array printed on a grounded dielectric substrate. The periods along the x- and y- directions are the same, and denoted as d. The sizes of the patches vary along the x-axis, but remain the same along the y-direction. The dimensions of the square patches along the x-direction are respectively denoted as a1, a2, a3, a4, and a5.

To understand the reflection characteristics of the gradient AMC surface, the full-wave simulation based on time-domain finite integration method (CST microwave studio) was employed to calculate the far-field scattering pattern. Figure 4 illustrates how the gradient AMC surface was placed inside a rectangular box equipped with absorbing boundary conditions. Excitation was performed by a normally incident plane wave with the electric- and magnetic field along the y- and x-axes, respectively.

Figure 5(a)–5(d) depicts the far-field reflection pattern on the x-z plane for the structure consisting of one, two, three, and six periods along the x-axis, respectively. The structure for CST simulation is attached in each figure. The vertical- and horizontal polarization denoted in the figure represent that the incident electric field is along the y and x axes, respectively. The reflection main beam is steered away from the normal incident direction. Although not shown here, some space left between the AMC surface and absorbing boundaries contributes to forward scattering. The scattering pattern demonstrated above produces an artificial surface that is able to reflect the incident energy away from the incident direction. As shown below, the commonly used array antenna formula can be used to determine the far-field scattering pattern. Furthermore, the 1D periodic structure composed of several cells, each of which contains a gradient AMC surface shown previously, was constructed to study the scattering characteristics of the cells. Figures through 5(b) to 5(d) show that the reflection main-beam angle swings and the beam-width became narrower as the period number increased. Besides, the grating lobes are apparent for the periodic gradient AMC surfaces. Notably, due to the square unit cell and patch, both states of polarization can excite a progressive phase shift in the linear array. However, the reflection electric fields of the two states are orthogonal to each other.

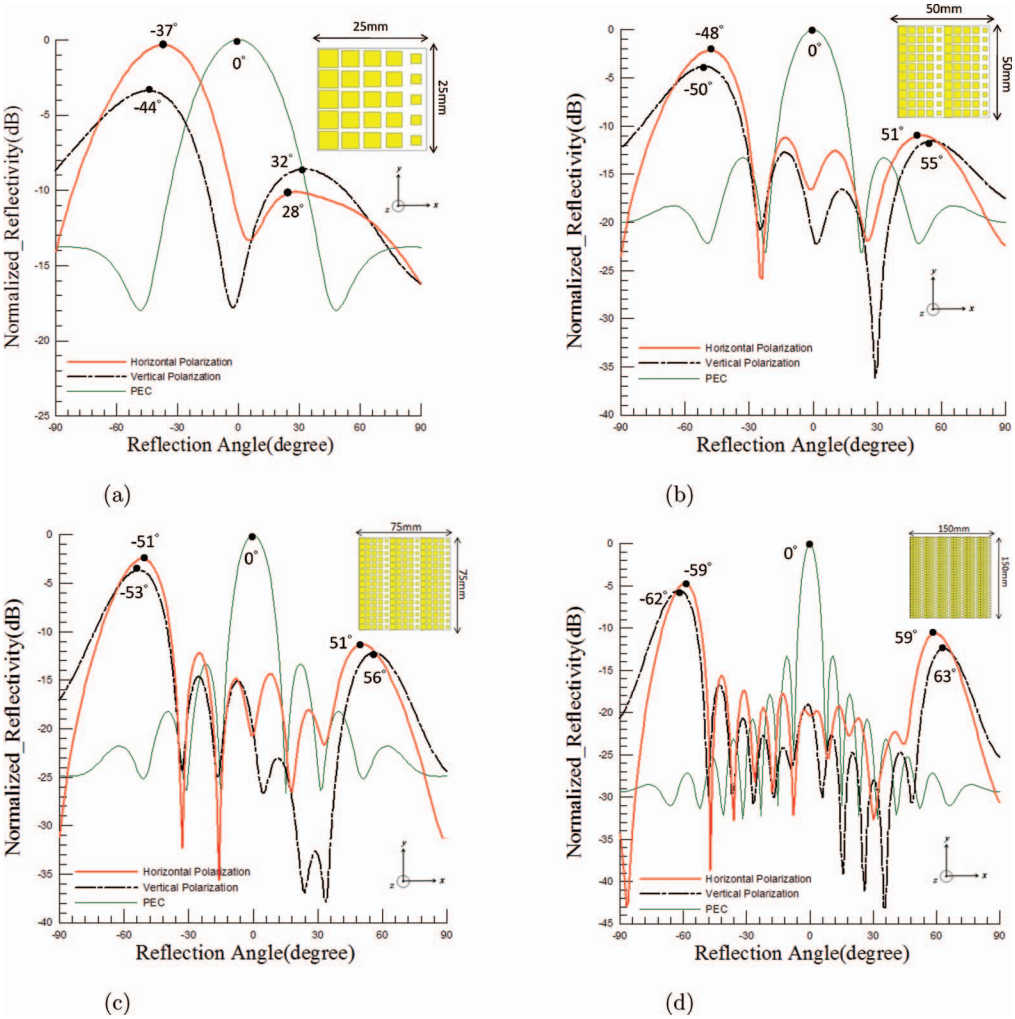

FIG. 5. Far-field reflection pattern for a periodic gradient AMC surface consisting of (a) one period, (b) two periods, (c) three periods, and (d) 6 periods, along the x-axis at 15GHz.

In addition to the far-field scattering pattern, this study calculates the reflection phase distribution on the plane with a distance 0.5 mm above the gradient AMC surface. The purpose of the near field scanning is to find out the phase distribution of the reflected wave over the AMC surface. Such information can be employed to estimate the scattering main-beam angle in the far field. From the numerical simulation results, on the AMC surface, the reflected amplitude of the first 4th higher-order space harmonics are smaller than that of the fundamental one. Moreover, these higher-order space harmonics are exponentially decaying in the air. We may conclude that the effect of the evanescent space harmonics on the radiation far-field pattern is insignificant. The horizontal axis represents the position along the x-axis indicated in the inset of Fig. 6, while the vertical axis is the reflection phase angle in degree. Significantly, the phase angles at the center position of each square patch are about 140°, 70°, 0°, −70°, and −140° respectively. According to array antenna theory, an antenna array with the progressive phase shift radiates its main beam toward the direction away from the broadside. This may explain the beam-steering characteristic of the reflection wave in Fig. 5(a).

IV. APPLICATION OF A COMPOSITE AMC SURFACE IN RCS REDUCTION

The scattering characteristics depicted above indicate that a gradient AMC surface can reflect the normally incident wave away from the incoming direction. This unique characteristic holds great

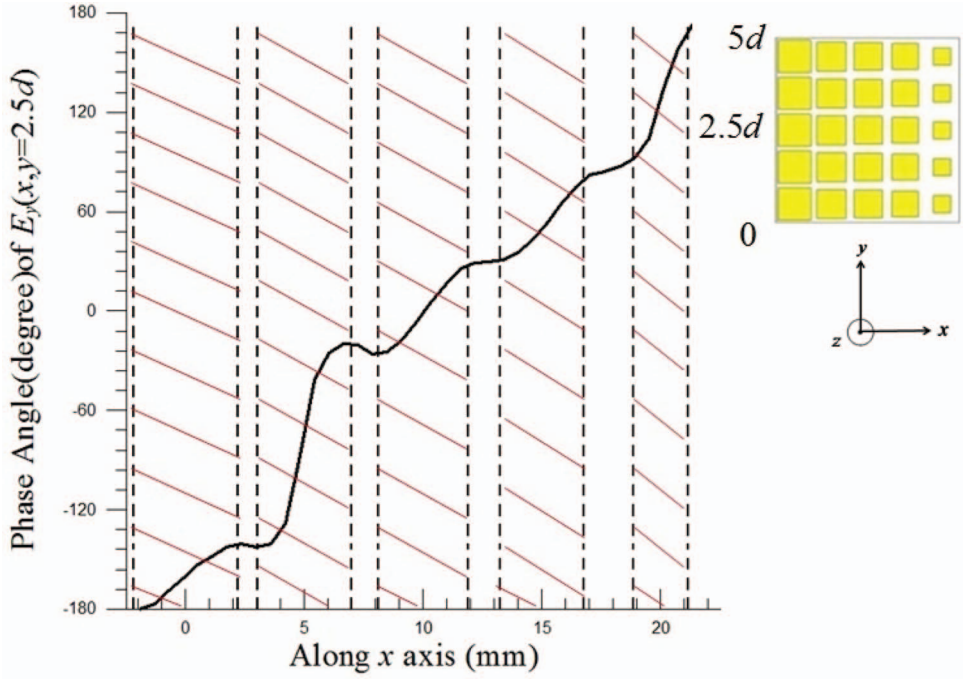

FIG. 6. Reflection phase of the Ey(x, y = 2.5d) against the position along the x-axis at 15GHz.

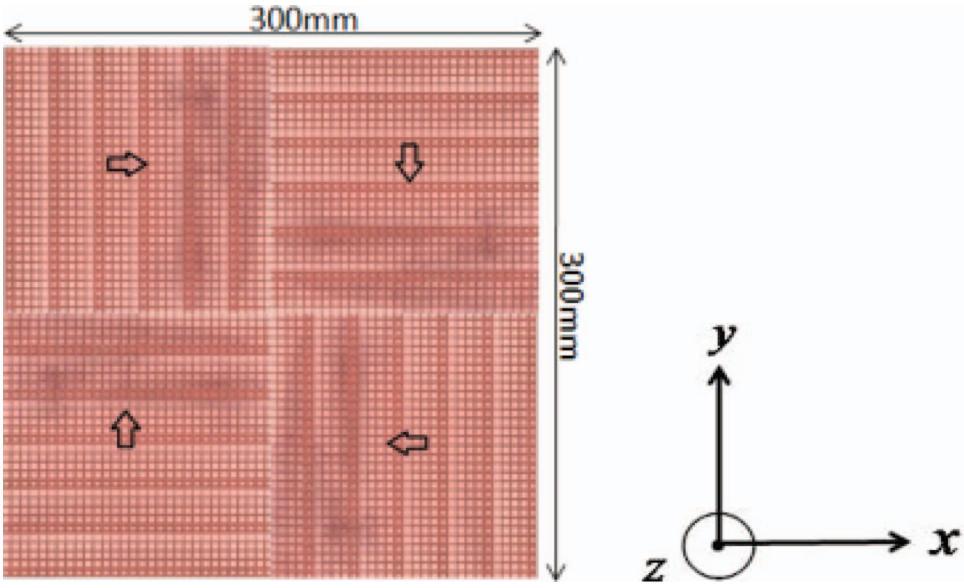

FIG. 7. A composite AMC surface consists of orthogonal gradient surfaces, the arrow attached in this figure represent the gradient direction.

promise for RCS reduction applications. However, previous designs steer the reflection beam on the x-z plane only. The performance of RCS reduction can be further improved if the incident energy can be distributed away from the incident direction into beams on both x-z and y-z planes. This section designs a composite AMC surface made up of orthogonal gradient AMC surfaces, as Fig. 7 shows. For numerical simulation, the entire structure was placed in a box with the absorbing boundary conditions to calculate the scattering far-field pattern of the structure illuminated by a normally incident plane wave (with electric field along the y-axis). Figure 8 shows the 3D scattering pattern

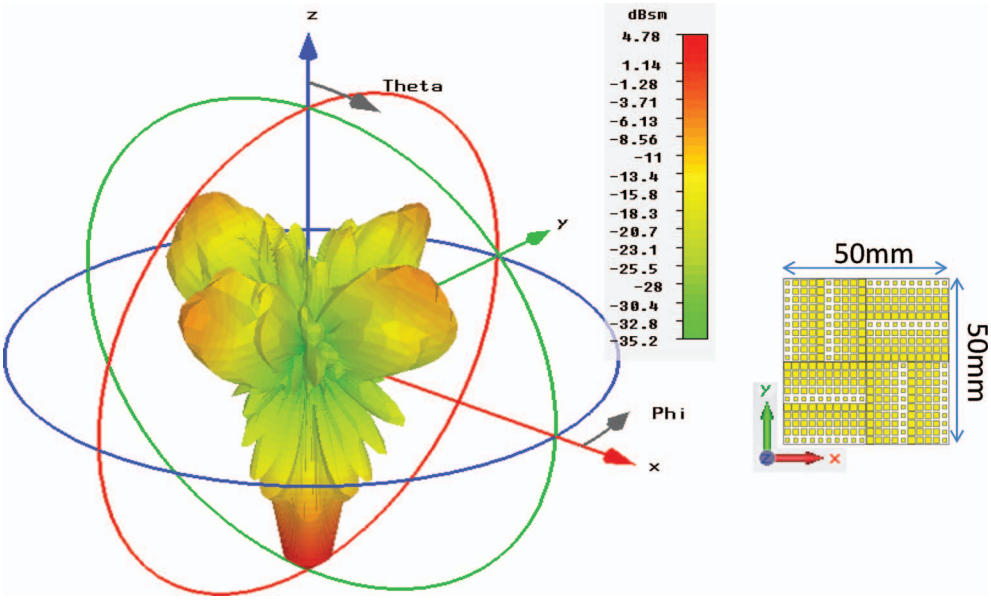

FIG. 8. 3D scattering pattern of a 50mmx50mm orthogonal gradient AMC surface illuminated by a normal incident plane wave with the electric field along the y-axis at 15GHz.

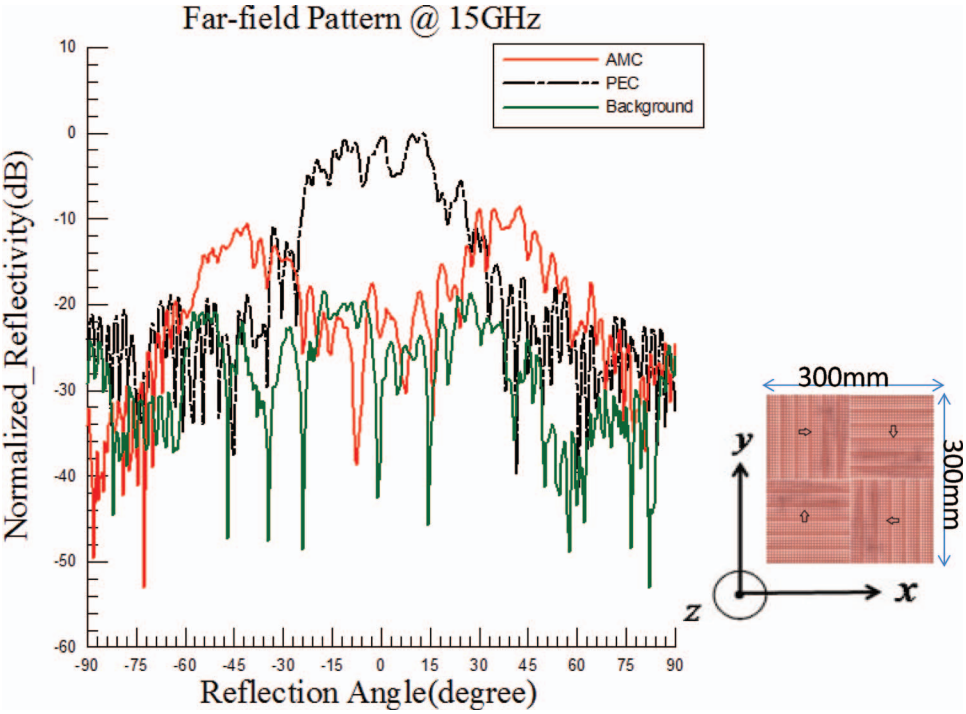

FIG. 9. Bi-static reflectivity versus elevation angle in degree on the x-z plane of the 300mmx300mm composite AMC surface at 15 GHz.

of a 50mm by 50mm orthogonal gradient AMC surface. The two major beams along the x-axis are contributed by the two gradient surfaces located at the upper-left and lower-right sub-surfaces. Note that due to the square pattern of the unit cell and its metal patches, the vertical polarization can also excite the two gradient surfaces at the upper-right and lower-left sub-surfaces, generating two major beams along the y-axis, but with the electric field vector along the y-axis.

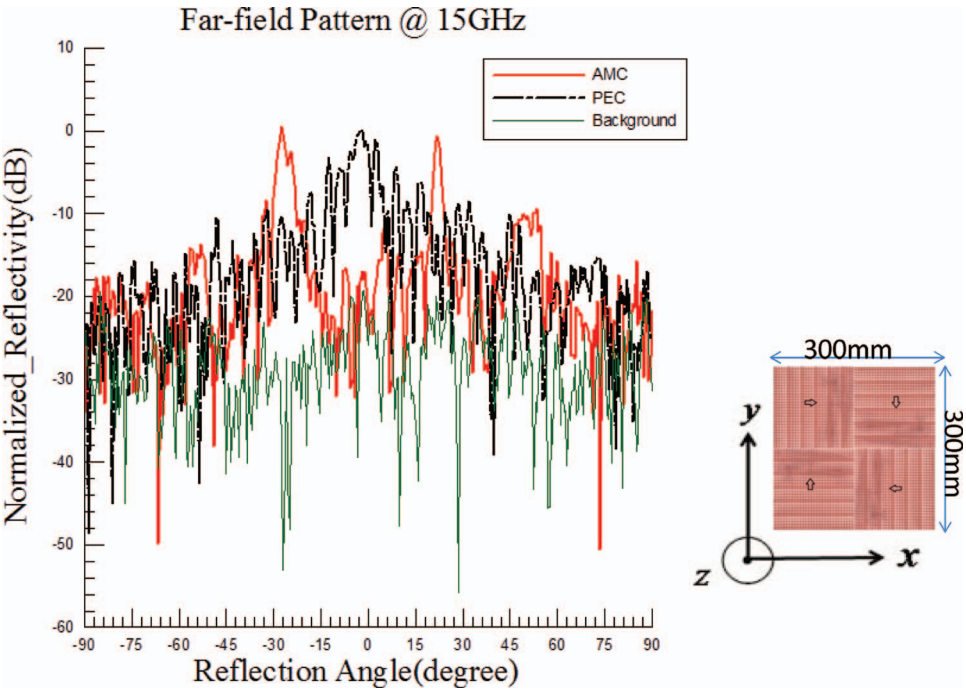

FIG. 10. Mono-static reflectivity versus elevation angle in degree on the x-z plane of the 300mmx300mm composite AMC surface at 15 GHz.

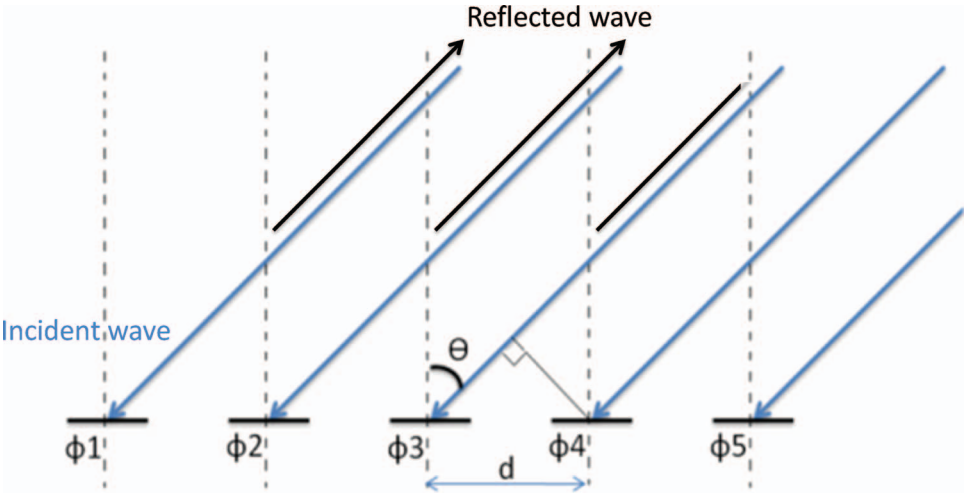

FIG. 11. The reflected waves from a period of gradient surface satisfying constructive interference condition.

In addition to the numerical calculation, this study reports the fabrication of a composite AMC structure and measures its bi-static and mono-static reflections. Measurements were carried out in an electromagnetic chamber using a vector network analyzer and standard gain horn antennas. Before measuring the reflection characteristic of the composite AMC surface, the scattering characteristic of the background (absorber reflectance) was first measured to identify the scattering sources. The reflection characteristic of an equal size metal plate was measured as a reference to determine the RCS reduction level for the composite AMC surface in the normal direction. Figure 9 show the reflection far-field pattern for a frequency of 15 GHz. The horizontal and vertical axes respectively represent the elevation angle in degrees and normalized reflectivity in dBs. The red, black, and green lines respectively represent the reflectivity of the composite AMC surface, PEC surface, and background.

Generally speaking, the composite AMC surface can reflect incoming waves away from the normal direction. Most of their energy will be scattered at approximately $\pm 45^\circ$. This study defines the RCS suppression rate based on the difference in the reflectance between those from the composite AMC and PEC surfaces. The average difference is calculated within the 3dB beam width of the receiving horn antenna. The RCS suppression rate for those frequencies is generally more than 10 dB. Additionally, Fig. 10 shows the mono-static reflectivity of the composite AMC surface. This study only demonstrates one figure, as the other frequencies share similar properties. The reflectivity of the composite AMC surface is more than 15 dB lower than that of the PEC surface near normal incidence. This means that the mono-static RCS suppression rate using the composite AMC is up to 15 dB. The peaks appearing around $+24^\circ$ and -27° are due to the reflected waves from the gradient surface of each period satisfying the constructive interference condition during mono-static reflectivity measurement, as Fig. 11 demonstrates. The peak of the reflected beam occurs at the angle when

$$\psi = 2k_0 d\sin\theta + \Delta\varphi = 0 \tag{3}$$

In this example, under oblique incidence, the reflected phase of each element will not be the same as the normal incidence condition obtained by the unit cell approach, and the difference in reflection phase between adjacent patches will become $\triangle\varphi = 77^\circ$. For distance d=5mm and operational frequency 15GHz, the angle, for constructive interference is approximately 25°, which is near the measured result shown in Fig. 10.

V. CONCLUSION

This study theoretically and experimentally investigates the reflection characteristic of a composite AMC surface. By adjusting the dimensions of the metal patches, it is possible to obtain a surface with the progressive phase shift in its reflection wave front to reflect the incident wave away from the impinging direction. Additionally, the orthogonal gradient AMC sub-surfaces were organized periodically and assembled in a surface to achieve four-beam splitting. Numerical and experimental studies confirm the excellent performance of this design in RCS reduction for both mono-static and bi-static reflections.

ACKNOWLEDGMENTS

We acknowledge with gratitude the support by the National Science Council under the contract number NSC100-2221-E-009-138.

[1] D. Sievenpiper, L. Zhang, R. F. J. Broas, N. G. Alexopoulos, and E. Yablonovitch, IEEE Trans. Microwave Theory Tech **47**, 2059 (1999).
[2] W. Yang, G. Hua, and W. Hong, Microwave, Antenna, Propagation and EMC Technologies for Wireless Communications, 2009 3rd IEEE International Symposium on, 954 (2009).
[3] D. J. Kern, D. H. Werner, A. Monorchio, L. Lanuzza, and M. J. Wilhelm, IEEE Trans. Antennas Propag. **53**, 8 (2005).
[4] M. Paquay, J. Iriarte, I. Ederra, R. Gonzalo, and P. de Maagt, IEEE Trans. Antennas Propag. **55**, 3630 (2007).
[5] Y. Zhang, R. Mittra, B.-Z. Wang, and N. V. Huang, Electronics Letters **45**, 484 (2009).
[6] S. Simms and V. Fusco, Electronics Letters **44**, 316 (2008).
[7] S. Simms and V. Fusco, Electronics Letters **42**, 1197 (2006).
[8] D. F. Sievenpiper, J. H. Schaffner, H. J. Song, R. Y. Loo, and G. Tangonan, IEEE Trans. Antennas Propag. **51**, 2713 (2003).
[9] D. Sievenpiper, J. Schaffner, J. J. Lee, and S. Livingston, IEEE Antenna and Wireless Propagation Letters **1**, 179 (2002).
[10] C. Mias and J. H. Yap, IEEE Trans. Antennas Propag. **55**, 1955 (2007).
[11] D. G. Berry, R. G. Malech, and W. A. Kennedy, IEEE Trans. Antennas Propag. **11**, 645 (1963).
[12] D. M. Pozar and T. A. Metzler, Electron. Lett., 657 (1993).
[13] J. Huang and R. J. Pogorzelski, IEEE Trans. Antennas Propag. **46**, 650 (1998).